The Hopf-saddle-node bifurcation for fixed points of 3D-diffeomorphisms: the Arnol'd resonance web

Henk Broer Carles Simó Renato Vitolo

Abstract

A model map Q for the Hopf-saddle-node (HSN) bifurcation of fixed points of diffeomorphisms is studied. The model is constructed to describe the dynamics inside an attracting invariant two-torus which occurs due to the presence of quasi-periodic Hopf bifurcations of an invariant circle, emanating from the central HSN bifurcation. Resonances of the dynamics inside the two-torus attractor yield an intricate structure of gaps in parameter space, the so-called Arnol'd resonance web. Particularly interesting dynamics occurs near the multiple crossings of resonance gaps, where a web of hyperbolic periodic points is expected to occur inside the two-torus attractor. It is conjectured that heteroclinic intersections of the invariant manifolds of the saddle periodic points may give rise to the occurrence of strange attractors contained in the two-torus. This is a concrete route to the Newhouse-Ruelle-Takens scenario. To understand this phenomenon, a simple model map of the standard two-torus is developed and studied and the relations with the starting model map Q are discussed.

1 Introduction

Recently, there has been renewed interest in certain codimension two (local) bifurcations of fixed points of diffeomorphisms. See [8, 15, 16, 17, 26] and references therein. Among these, the Hopf-saddle-node (HSN) bifurcation for 3D diffeomorphisms is defined as follows: let $F_\alpha : \mathbb{R}^3 \to \mathbb{R}^3$ be a C^∞-family of diffeomorphisms, where $\alpha \in \mathbb{R}^p$

2000 *Mathematics Subject Classification :* 34K18, 37D45, 35B34.

Key words and phrases : Quasi-periodic bifurcations; Invariant two-torus; Ruelle-Takens scenario.

is a multi-parameter. We say that F_α is an *HSN-family of diffeomorphisms* if

$$F_0(0) = 0, \quad \text{and} \quad \operatorname{spec} DF_0(0) = \{e^{i\omega_0}, e^{-i\omega_0}, 1\}, \tag{1}$$

where the complex conjugate eigenvalues satisfy the non-resonance conditions

$$e^{in\omega_0} \neq 1 \qquad \text{for} \quad n = 1, 2, 3, 4. \tag{2}$$

The values $n = 1, 2, 3, 4$ in (2) are the so-called strong resonances [1, 14, 24]: they are excluded since, for those values, the contribution of resonant terms appears in the 3-jet. Moreover, to have a HSN bifurcation, one must impose certain generic conditions on the 3-jet of the map F, including a transversality condition for the unfolding of the linear part DF of the map at the origin, see [8].

In [8] we construct and study a model family of 3D maps for the HSN bifurcation of fixed points near a 1:5 resonance, which is the lowest order resonance compatible with (2). Due to the construction of the model map, a quasi-periodic Hopf bifurcation of invariant circles occurs, where an invariant circle loses stability, turning from an attractor into a repellor, and a two-torus attractor shows up. Particular attention is devoted to the intricate bifurcation structure existing near a 1:5 resonance 'bubble' on the locus of quasi-periodic Hopf bifurcations.

In the present paper, we examine the structure of the parameter space induced by the occurrence of resonant dynamics inside the two-torus attractors, further away from the quasi-periodic Hopf bifurcation. To this purpose, we study a parametrised family Q of maps, given by

$$Q : \begin{pmatrix} x \\ y \\ z \end{pmatrix} \mapsto \begin{pmatrix} \operatorname{Re}\left(e^{i\omega}(x+iy)[1-\gamma(\gamma\mu + az + \gamma z^2)]\right) \\ \operatorname{Im}\left(e^{i\omega}(x+iy)[1-\gamma(\gamma\mu + az + \gamma z^2)]\right) \\ z + \gamma(1 - x^2 - y^2 - z^2) \end{pmatrix} + \begin{pmatrix} \gamma^3\varepsilon_1(y^4 + z^4) \\ \gamma^3\varepsilon_2(x^4 + z^4) \\ \gamma^3\varepsilon_3(x^4 + y^4) \end{pmatrix}. \tag{3}$$

The family Q depends on the three real parameters (γ, μ, ω) and is given in the real coordinates $(x, y, z) \in \mathbb{R}^3$. The coefficients $a = a_1 + ia_2 \in \mathbb{C}$ and $\varepsilon_j \in \mathbb{R}$, $j = 1, 2$ are constants which are assumed to belong to a fixed compact set. The present paper contains a summary of results concerning model map Q, mostly obtained by numerical means.

An outline of this paper follows. In Sec. 2, in order to clarify the purpose of map Q we sketch its construction, referring to [26, Sec. 4.1.2] and to [8] for details. Then a description of some of the dynamical phenomena observed for Q is given in Sec. 3. In Sec. 4 we study a simple map defined on the standard two-torus, aimed at modelling and understanding the behaviour of Q, and describe the regular-chaotic transitions. Then in Sec. 5 we look, in the original map Q, for phenomena similar to those of the simple model map. Open problems and future research lines are discussed in Sec. 6.

2 Model construction and purpose

The construction of model map Q in (3) is here only sketched, since it follows the same steps as in [8], also see [26, Sec. 4.1.2] for details. The starting point is a version of Takens's Theorem [24] which allows to approximate any HSN family

of diffeomorphisms by the time-one map of a HSN family of vector fields. To be precise, let $F : \mathbb{R}^3 \times \mathbb{R}^p \to \mathbb{R}^3 \times \mathbb{R}^p$ be a HSN family of diffeomorphisms such that conditions (1) and (2) hold for F_α defined by $F(x, \alpha) = (F_\alpha(x), \alpha)$, $x \in \mathbb{R}^3$ and $\alpha \in \mathbb{R}^p$. Then there exists a vector field T_F defined on $\mathbb{R}^3 \times \mathbb{R}^p \to \mathbb{R}^3 \times \mathbb{R}^p$ such that

$$F = T_F^1 + M, \tag{4}$$

where T_F^1 denotes the time-one map of the flow of T_F and the 3-jet of M at the origin is zero. Moreover, T_F is an HSN family of vector fields (see [8, Theorem 1] for the definition and the proof of (4)). A truncated simplified normal form for vector fields having an HSN bifurcation of equilibria is the following:

$$Y_{\beta_1,\beta_2,\omega}(w, z) = \begin{pmatrix} (-\beta_2 + i\omega)w - awz - wz^2 \\ -\beta_1 - sw\overline{w} - z^2 \end{pmatrix}, \tag{5}$$

see [14, Lemma 8.11] and [8, Lemma 6]. Here $(\beta_1, \beta_2, \omega)$ are real parameters, whereas $w = x+iy \in \mathbb{C}$ and $z \in \mathbb{R}$ are the phase variables and $a = a_1+ia_2 \in \mathbb{C}$ is a constant. Typically, for the analysis of vector fields time scalings are allowed, since one works modulo orbital equivalence; therefore, ω is usually considered as a nonzero constant. In our case, however, the parameter ω plays a very important role in connection with resonances in the dynamics on invariant circles and invariant two-tori.

Briefly speaking, the construction of model map Q (3) runs as follows: we start from the vector field $Y_{\beta_1,\beta_2,\omega}$ in (5), apply a parameter transformation and a rescaling of time and variables, compute an (approximate) time-1 map, and add certain perturbative terms of order four. By (4), this construction is likely to be representative for a large class of HSN-diffeomorphisms. We emphasise that our construction focuses on dynamical phenomena occurring in a specific region of the (β_1, β_2)-parameter plane for one of the four possible unfolding types of $Y_{\beta_1,\beta_2,\omega}$. Therefore, to clarify our setting we briefly recall the bifurcation diagram of the vector field $Y_{\beta_1,\beta_2,\omega}$. Since the latter is axially symmetric, a planar reduction may be derived:

$$\begin{aligned} \dot{r} &= r(-\beta_2 - a_1 z - z^2), \\ \dot{z} &= -\beta_1 - z^2 - sr^2, \end{aligned} \tag{6}$$

where a_1 is the real part of the coefficient a in (5). According to the signs of s and a_1, the topological structure of the phase portrait of the reduced system (6) belongs to one of four classes (if a time-reversal is allowed [14]). The unfolding case of present interest is ($s = 1$, $a_1 < 0$), for which both Hopf and heteroclinic bifurcations occur. The bifurcation diagram of the planar system (6) consists of the curves $\mathcal{S}$, $\mathcal{P}$, $\mathcal{H}$, which are saddle-node, pitchfork, and (Andronov-)Hopf bifurcations of equilibria, respectively, and $\mathcal{HET}$ which is a curve of heteroclinic bifurcations of equilibria, see Figure 1. Two 'polar' equilibria $\mathscr{O}_\pm = (\pm\sqrt{-\beta_1}, 0)$, both of saddle type, exist in regions 2 up to 6. Furthermore, a third equilibrium $\mathscr{C}$ coexists with $\mathscr{O}_\pm$ in regions 3, 4, 5. The equilibrium $\mathscr{C}$ is attracting in region 3 and repelling in regions 4 and 5. Entering region 4 from region 3 across curve $\mathcal{H}$, the equilibrium $\mathscr{C}$ loses stability through a Hopf bifurcation. Thereby, an attracting limit cycle $\mathscr{T}$ is created, which persists throughout region 4.

The dynamics of the three-dimensional family $Y_{\beta_1,\beta_2,\omega}$ is easily reconstructed from that of the planar reduction (6). The equilibria $\mathscr{O}_\pm$ of (6) correspond to

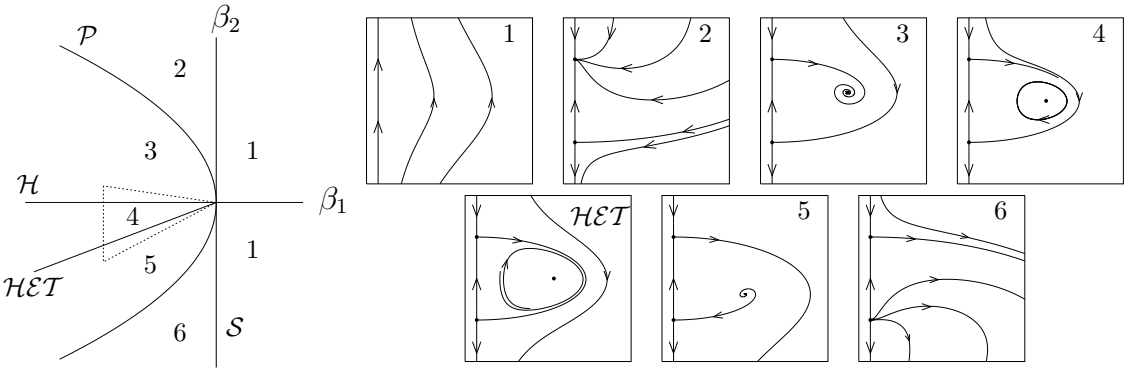

Figure 1: Unfolding of the HSN bifurcation for vector fields: bifurcation diagram of the planar system (6) in the case $s = 1$, $a_1 < 0$, from [14, §8.5]. Phase portraits in the (r, z)-plane are given on the right.

equilibria of $Y_{\beta_1,\beta_2,\omega}$ belonging to the z-axis. On the curve $\mathcal{P}$ the equilibrium $\mathscr{O}_+$ loses stability through a Hopf bifurcation, and a limit cycle $\mathscr{C}$ is created. Across curve $\mathcal{H}$, the limit cycle $\mathscr{C}$ loses stability through a Neĭmark-Sacker [14] bifurcation, where an attracting torus $\mathscr{T}$ is created. Then $\mathscr{T}$ merges into a heteroclinic sphere-like structure on the curve $\mathcal{HET}$ and disappears.

Due to non-degeneracy of the Hopf bifurcation, the curve $\mathcal{H}$ is expected to persist in any HSN family of vector fields X_α, $\alpha \in \mathbb{R}^2$, which can be written as a perturbation of $Y_{\beta_1,\beta_2,\omega}$ (modulo changes of variables and parameters and orbital equivalence). Therefore, there exists a parameter domain characterised by the existence of a normally hyperbolic attracting two-torus of X_α. Loosely speaking, such domain is the dynamical equivalent of region 4 in Figure 1 for X_α. However, the so-called Arnol'd resonance 'tongues' appear in the parameter plane, with tips attached to $\mathcal{H}$ and extending into the region of existence of the normally hyperbolic torus. For α in the interior of such tongues, the two-torus is *phase-locked*: there exists a pair of limit cycles, to be denoted as $\mathscr{L}_a$ and $\mathscr{L}_s$, such that $\mathscr{L}_a$ is an attractor, $\mathscr{L}_s$ is of saddle type, and

$$\mathscr{T} = \mathscr{L}_a \cup W^u(\mathscr{L}_s), \tag{7}$$

where $W^u(\mathscr{L}_s)$ denotes the unstable manifold of $\mathscr{L}_s$. In this case, generically the two-torus is only finitely differentiable (see [6, 7] for a similar situation). Further away from the Hopf curve $\mathcal{H}$, the torus might lose its smoothness and even get destroyed. This sort of dynamical phenomena has a counterpart in families of diffeomorphisms having a HSN bifurcation. Main focus of this paper is to try to understand (some of) the corresponding bifurcation patterns. Before discussing the generic expectations for diffeomorphisms, however, we briefly sketch the construction of model map Q (3).

We start from vector field $Y_{\beta_1,\beta_2,\omega}$ (5), in the unfolding case $a_1 < 0$, $s = 1$. The area of interest in the (β_1, β_2)-parameter plane is bounded by a dashed triangle in Figure 1 (left panel): it is a sector containing region 4 and parts of regions 3 and 5. Only negative values of β_1 are considered. New parameters (γ, μ) are introduced by

$$\beta_1 = -\gamma^2, \quad \beta_2 = \gamma^2\mu, \tag{8}$$

where $\gamma > 0$ and $\mu \in \mathbb{R}$. The effect of this reparametrisation is to 'blow-up' the dashed sector in Figure 1 near the origin. Moreover, the variables and the time

of (5) are rescaled as follows:

$$w = \gamma\widehat{w}, \quad z = \gamma\widehat{z}, \quad t = \widehat{t}/\gamma. \tag{9}$$

The effect of this scaling is to keep the sizes of the limit cycle $\mathscr{C}$ and of the torus $\mathscr{T}$ of order $\mathcal{O}(1)$ as $\gamma \to 0$. In the new variables and parameters, dropping all hats, the vector field in (5) reads

$$Y_{\gamma,\mu,\omega} = \begin{pmatrix} (-\gamma\mu + i\omega/\gamma)w - awz - \gamma w z^2 \\ 1 - z^2 - |w|^2 \end{pmatrix}. \tag{10}$$

We obtain an approximate time-γ map of the vector field $Y_{\gamma,\mu,\omega}$ by performing one step of length γ of the Euler integration formula. This yields the axially symmetric map S:

$$S : \begin{pmatrix} w \\ z \end{pmatrix} \mapsto \begin{pmatrix} e^{i\omega}w[1 - \gamma(\gamma\mu + az + \gamma z^2)] \\ z - \gamma(-1 + |w|^2 + z^2) \end{pmatrix}. \tag{11}$$

Note that this map is the first term in the right hand side of (3). The second and last step of the construction is to add 'generic', non-axisymmetric terms of order four to map S. In [8], since we restricted to a neighbourhood of the 1:5 resonance, we chose suitable resonant terms of order four. In the present work, since we intend to examine a wide interval for ω, we do not confine ourselves to the vicinity of a specific resonant frequency. Therefore, we introduce the perturbation term

$$\gamma^3\varepsilon_1(y^4 + z^4)\frac{\partial}{\partial x} + \gamma^3\varepsilon_2(x^4 + z^4)\frac{\partial}{\partial y} + \gamma^3\varepsilon_3(x^4 + y^4)\frac{\partial}{\partial z}, \tag{12}$$

where $\varepsilon_j \in \mathbb{R}$, $j = 1, 2, 3$, which yields (3). The purpose of adding such perturbation term is to have higher order terms in Q which are 'generic', in the sense that they contain monomials which are resonant with respect to ω for 'many' resonant values of ω. The coefficients ε_j and γ are perturbation parameters. However, we shall treat them as constants in the rest of this paper.

We now sketch our generic expectations for model map Q (3). Referring to Figure 1, for parameters in the interior of region 4 the vector field $Y_{\beta_1,\beta_2,\omega}$ (5) possesses an invariant two-torus $\mathscr{T}$ which is normally hyperbolic and attracting. The winding number on $\mathscr{T}$ might be rational or irrational: in the first case, one has (generically) a phase-lock configuration as in (7). By construction and by normal hyperbolicity, in suitable regions of the parameter space (γ, μ, ω) the limit cycle $\mathscr{C}$ and the two-torus $\mathscr{T}$ of the vector field $Y_{\gamma,\mu,\omega}$ (10) are expected to persist as a normally hyperbolic invariant circle and a two-torus, respectively, for map Q (and are denoted by the same symbol). By quasi-periodic bifurcation theory [4, 3], the Hopf bifurcation curve $\mathcal{H}$ of vector field $Y_{\gamma,\mu,\omega}$ turns into a frayed Cantor-like bifurcation boundary for map Q (as well as for any map obtained by generic perturbation of the time-γ map of $Y_{\gamma,\mu,\omega}$). Roughly speaking, by crossing $\mathcal{H}$ along curves in parameter plane such that the circle attractor $\mathscr{C}$ has a fixed, Diophantine rotation number, $\mathscr{C}$ loses stability and the torus attractor $\mathscr{T}$ branches off. The Cantor-like Hopf boundary $\mathcal{H}$ is interspersed by resonance 'bubbles' where either the circle or the torus (or both) may cease to exist: the main goal of [8] was to understand the bifurcation scenarios involved near the 'bubbles' along $\mathcal{H}$. In the present paper we focus on the dynamics

inside the two-torus $\mathscr{T}$ of map Q, away from $\mathcal{H}$. As opposed to the vector field case, *two types* of resonances are possible: one type is related to the fast 'longitudinal' rotation and the other to the relatively slow 'latitudinal' rotation. Either type occurs in tongue-shaped regions in the (γ, μ, ω)-parameter space, having all kinds of orientations. The pattern formed by these resonance tongues is referred to as the Arnol'd resonance web. The related bifurcation scenarios are the main point of interest of the present paper.

We note that the dynamics on the two-torus can be resonant in two different ways: either *simple resonance*, giving rise to attracting and repelling invariant circles on the invariant torus, or *double resonance*, when the dynamics along invariant circles becomes in turn phase locked (for one or several of the circles). The last case produces the apparition of periodic points on the torus. The relative position of the manifolds of these hyperbolic periodic points can originate complicated dynamics, to be discussed in the next sections.

The choice of Euler's explicit method to go from the flow of (10) to map (11) is particularly relevant for the structure of the resonance gaps. To understand why, consider a planar conservative linear system like $\dot{x} = ax + by$, $\dot{y} = cx - ay$. The map induced by Euler's method with step size γ is linear and its matrix has determinant $1-(a^2+bc)\gamma^2$. Therefore, the numerical method produces an expansive (respectively, dissipative) map in the case that the origin is a centre (respectively, a saddle). Other integration methods have different behaviour around these points or the determinant differs from 1 by $O(\gamma^k)$, $k > 2$. On the invariant torus of vector field $Y_{\gamma,\mu,\omega}$ the flow is close to conservative. When passing to the map we can have values of the parameters for which the two frequencies of the torus dynamics satisfy a double resonance condition, giving rise to periodic points as mentioned in last paragraph. Were the map exactly conservative in the torus, generically half of the periodic points would be centres and the other half would be saddles. Using Euler's method the centres always become unstable foci: in this way it is prevented that they become attractors. On the other hand the saddles become dissipative. If homoclinic tangles exist, this allows the possibility that strange attractors are created *inside* the surface of the torus. This would constitute a first concrete example of route to the Ruelle-Takens scenario [18, 19].

3 Two-torus dynamics: the Arnol'd resonance web

In this section we discuss the dynamics on the two-torus $\mathscr{T}$ of model map Q (3) by means of numerical simulations. Throughout the section, the coefficients of Q are fixed at the values $\varepsilon_1 = \varepsilon_2 = \varepsilon_3 = 1$, $a_1 = -1$, $a_2 = 1/\sqrt{2}$,. Moreover, the parameter γ is kept fixed at 0.1. throughout the rest of the paper: therefore, all results are presented and discussed in the (μ, ω)-parameter plane.

We begin by presenting a 'Lyapunov diagram' of Q in Figure 2 (top panel). The procedure followed to obtain the Lyapunov diagram is explained in [8, 23, 26]. Here it suffices to say that a fine grid in the parameter plane is scanned searching for attractors and, for all parameter values for which an attractor is detected, the Lyapunov exponents

$$\ell_1 \geq \ell_2 \geq \ell_3$$

colour	Lyapunov exponents	attractor type
red	$\ell_1 > 0 = \ell_2 > \ell_3$	strange attractor
yellow	$\ell_1 > 0 > \ell_2 > \ell_3$	strange attractor
blue	$\ell_1 = 0 > \ell_2 = \ell_3$	invariant circle of focus type
green	$\ell_1 = \ell_2 = 0 > \ell_3$	invariant two-torus
black	$\ell_1 = 0 > \ell_2 > \ell_3$	invariant circle of node type
grey	$0 > \ell_1 > \ell_2 = \ell_3$	periodic point of focus type
fuchsia	$0 > \ell_1 = \ell_2 \geq \ell_3$	periodic point of focus type
pale blue	$0 > \ell_1 > \ell_2 > \ell_3$	periodic point of node type
white		no attractor detected

Table 1: Legend of the colour coding for Figure 2: the attractors are classified by means of the Lyapunov exponents (ℓ_1, ℓ_2, ℓ_3). Note that attracting periodic points are almost never detected: no grey, fuchsia, or pale blue are distinguishable in Figure 2.

are computed. The attractors are then classified on the basis of ℓ_1, ℓ_2, ℓ_3 according to the colour coding specified in Table 1.

The Cantor-like Hopf bifurcation boundary $\mathcal{H}$ is visible as a vertical line near the value $\mu \approx 0.97$. This matches, with good approximation, with estimates obtained by analytical means for map S (11), see [8, Lemma 2]. The blue region at the right of the picture is a parameter domain where the invariant circle $\mathscr{C}$ exists and it is attracting and of focus type in the normal direction. At the left of $\mathcal{H}$, the two-torus $\mathscr{T}$ exists and it is attracting. Moreover, in the green regions $\mathscr{T}$ is quasi-periodic: both frequencies in its rotation vector are irrational and, moreover, they are not resonant with each other. Several tongue-shaped gaps emerge from $\mathcal{H}$ (at its left): these correspond to resonances inside the two-torus attractor. As said above, two types of resonances may occur on $\mathscr{T}$: one related to the fast 'longitudinal' rotation, and the other one related to the relatively slow 'latitudinal' rotation. Close to $\mathcal{H}$, the 'longitudinal' resonances are predominant in the parameter plane and may be identified with the tips of the tongue-shaped gaps. Further away from $\mathcal{H}$, these gaps intersect with each other, as well as with thinner gaps corresponding to 'latitudinal' resonances. This gives rise to a pattern which we refer to as the Arnol'd resonance web. An illustration of this web is given in Figure 2 (bottom panel), which is a magnification of Figure 2 (top).

Quasi-periodic saddle-node bifurcations of invariant circles [3, 4] bound each of the resonance gaps. At the gap boundaries we expect the whole range of phenomena described in [2, 10, 11, 12, 13, 10, 22, 25, 27, 28]. These quasi-periodic saddle-node bifurcations take place inside $\mathscr{T}$, in the sense that inside the gaps (at least for parameter values near the gap edges) the two-torus still persists and it is 'phase-locked': there exist invariant circles $\mathscr{L}_a$ and $\mathscr{L}_s$ (possibly, periodically invariant), where $\mathscr{L}_a$ is an attractor and $\mathscr{L}_s$ a saddle, such that $\mathscr{T} = \mathscr{L}_a \cup W^u(\mathscr{L}_s)$. This is the equivalent of (7) for diffeomorphisms. In the interior of a gap this phase-locked two-torus may cease to exist. One possibility is that $\mathscr{L}_a$ becomes of focus type (in

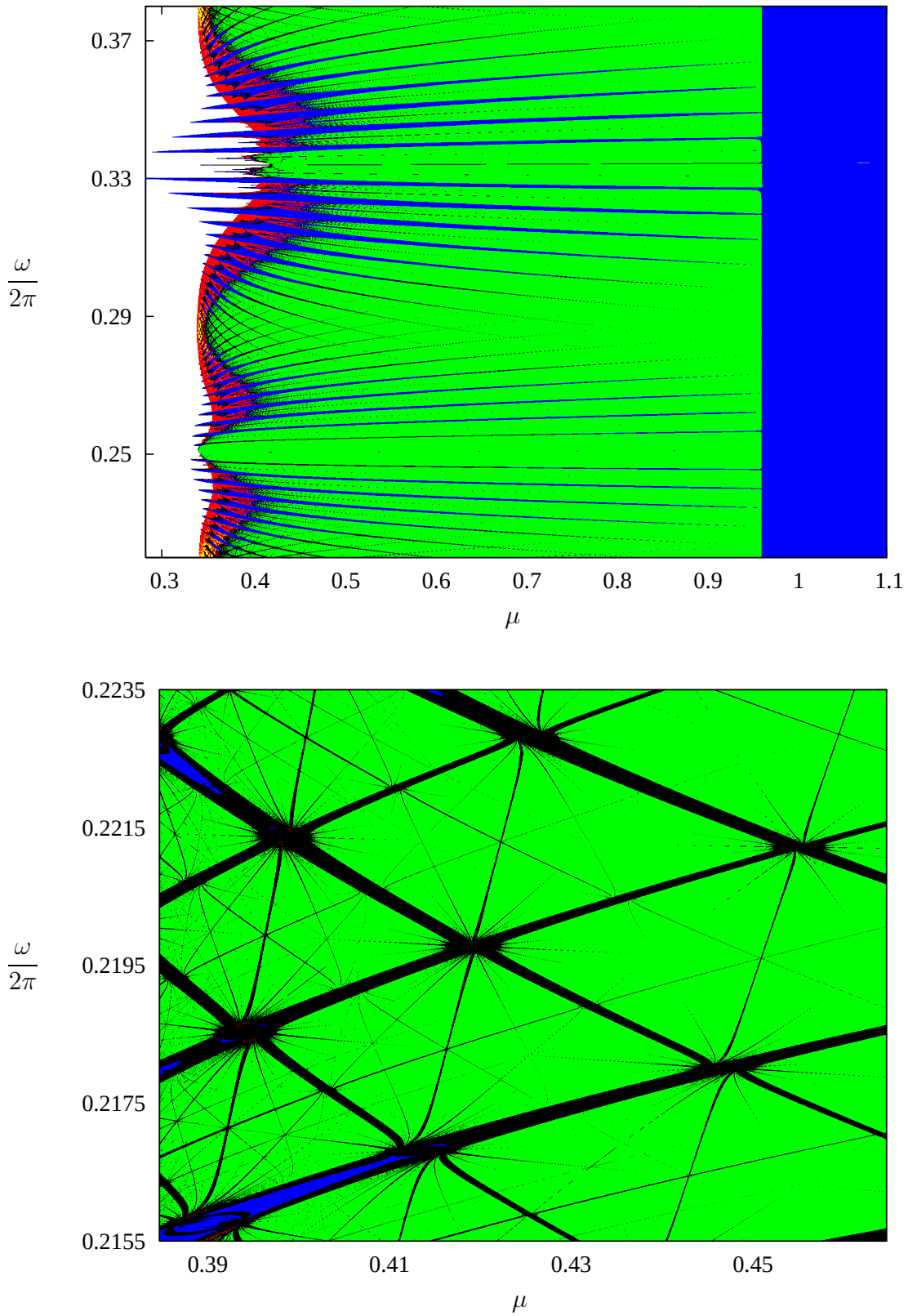

Figure 2: Top: Lyapunov diagram of the map Q in the $(\mu, \omega/(2\pi))$-parameter plane. For the colour code see Table 1. Bottom: magnification of top picture near a region characterised by several resonance gap crossings.

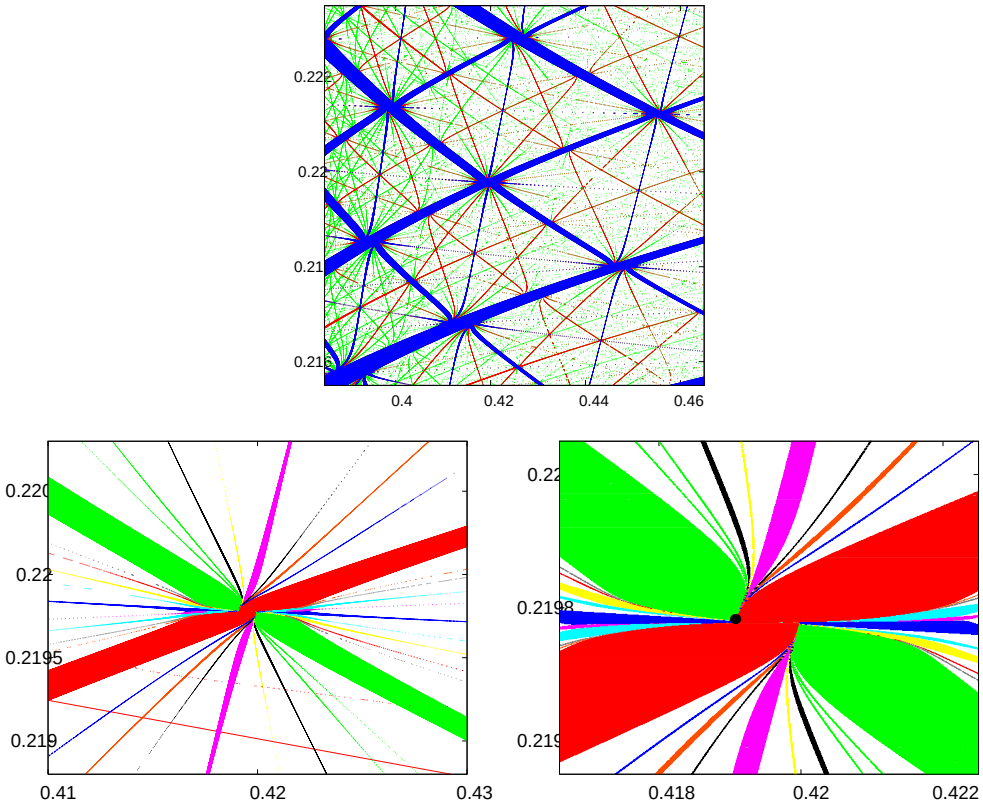

Figure 3: Top: the same parameter domain as in Figure 2 bottom is plotted, this time displaying the order of resonance inside $\mathscr{T}$. Colour coding: blue for resonances of order less than 22 (mainly in diagonal, almost horizontal or almost vertical strips), red for order between 22 and 62 and green for larger order. Bottom left: magnification of top plot near one of the resonance gap crossings. Parameter gaps with resonances of different orders (inside $\mathscr{T}$) are displayed in different colours. Bottom right: magnification of left. The black dot at the junction of the strips shows the approximate location of the parameter values at which the attractors $\mathscr{L}_{a,1}$ and $\mathscr{L}_{a,2}$ in Figure 4 and the attractors in Figure 8 occur.

the normal direction): thereby, the torus becomes a C^0-manifold. This is in fact observed in map Q: for example, a large part of the resonance gap near the lower left corner of Figure 2 (bottom) is coloured in blue, indicating the presence of an invariant circle of focus type (compare Table 1), whereas near the gap edges the same invariant circle is of node type (parameter region coloured in black). Another possibility for the destruction of the torus is the occurrence of a homoclinic tangency of the stable and unstable manifolds of $\mathscr{L}_s$: this is a generalisation of the dynamical scenarios described in [7], where the role of a periodic point of saddle type is played by the invariant circle $\mathscr{L}_s$. In this case, however, for nearby parameter values the circle attractor $\mathscr{L}_a$ still persists due to normal hyperbolicity. This scenario is more difficult to locate by numerical means.

A particularly rich structure exists near multiple 'crossings' of various resonance gaps. In Figure 3 (bottom panels) several resonance gaps are plotted near one of these crossings. Assume that for some initial condition on the invariant two-torus

the *rotation vector* (ρ_1, ρ_2) is defined, where ρ_1 and ρ_2 are the two rotation numbers in the longitudinal and latitudinal directions. Then a resonance occurs if

$$k_1\rho_1 + k_2\rho_2 + k_3 = 0 \tag{13}$$

for some $k_j \in \mathbb{Z}$ (not all of them equal to zero) and the order of the resonance is defined as $|k_1| + |k_2| + |k_3|$. At the crossing of the two large resonant strips in Figure 3 bottom the values of ρ_1, ρ_2 are close to $16/73$ and $1/73$, respectively. Resonances are associated to the solutions of the Diophantine equation $16k_1 + k_2 + 73k_3 = 0$. In Figure 3 bottom, the strip close to the diagonal of the first quadrant satisfies $(k_1, k_2, k_3) = (5, -7, -1)$, while for the diagonal of the second quadrant and for the near-horizontal and near-vertical strips the respective values are $(4, 9, -1), (1, -16, 0), (9, 2, -2)$. This exhausts the resonances of order less than 22 which appear in the (μ, ω)-parameter window in the bottom panels.

We stress that infinitely many gaps and gap crossings (associated to the solutions of Diophantine equation for double resonances) could be expected to occur near the boundary of any given gap. Correspondingly, the transition between two nearby gaps would imply infinitely many quasi-periodic saddle-node bifurcations. It is unclear if the existence of some very narrow gaps is prevented by the presence of gaps associated to resonances of lower order.

Moreover, sequences of heteroclinic tangency bifurcations of two saddle-like periodic points are involved in certain cases. The latter scenario is illustrated in Figure 4. Two attracting invariant circles $\mathscr{L}_{a,1}$ and $\mathscr{L}_{a,2}$, occurring at different parameter values, are plotted in Figure 4 top left and right, respectively. The bottom panel of the figure displays both invariant circles using the angles

$$\theta_1 = \arctan(y/x), \qquad \arctan(z/(\sqrt{x^2 + y^2} - b),$$

always in the correct quadrant and where b has been taken equal to $1/\sqrt{2}$. It is clearly seen that the circles nearly coincide along arcs which are roughly horizontal and separate near a saddle. As one can expect the saddles which seem to exist in the invariant two-torus have period 73.

A possible theoretical scenario for the transition from $\mathscr{L}_{a,1}$ to $\mathscr{L}_{a,2}$ is the following. The invariant two-torus $\mathscr{T}$ persists for all parameter values in a connected neighbourhood $\mathcal{N}$ of the two values for which $\mathscr{L}_{a,1}$ and $\mathscr{L}_{a,2}$ occur. Depending on the parameter values, the two-torus $\mathscr{T}$ is phase-locked either to $\mathscr{L}_{a,1}$, or to $\mathscr{L}_{a,2}$, or to neither of them. Consider the dynamics restricted to the two-dimensional surface given by the invariant two-torus $\mathscr{T}$. Two periodic orbits $P^{\pm}$ of saddle type occur on $\mathscr{T}$. In a narrow parameter subset of $\mathcal{N}$, the unstable manifold $W^u(P^+)$ and the stable manifold $W^s(P^-)$ have transversal heteroclinic intersections (and tangencies). When approaching the heteroclinic structure formed by $W^u(P^+) \cup W^s(P^-)$, the invariant circle $\mathscr{L}_{a,1}$ is destroyed. Then the circle $\mathscr{L}_{a,2}$ 'reappears' right after the region of heteroclinic intersections is crossed. A qualitative sketch is given in Figure 5 (A) and (B): both situations are obtained by perturbing the time-one map of an integrable vector field defined on the two-torus $\mathbb{S}^1 \times \mathbb{S}^1$, the dynamics of which is sketched in Figure 5 (C).

The above scenario is suggested by the 'swapping' between the 'vertical straight segments' of $\mathscr{L}_{a,1}$ and $\mathscr{L}_{a,2}$, as illustrated in Figure 4 bottom. Notice that there are

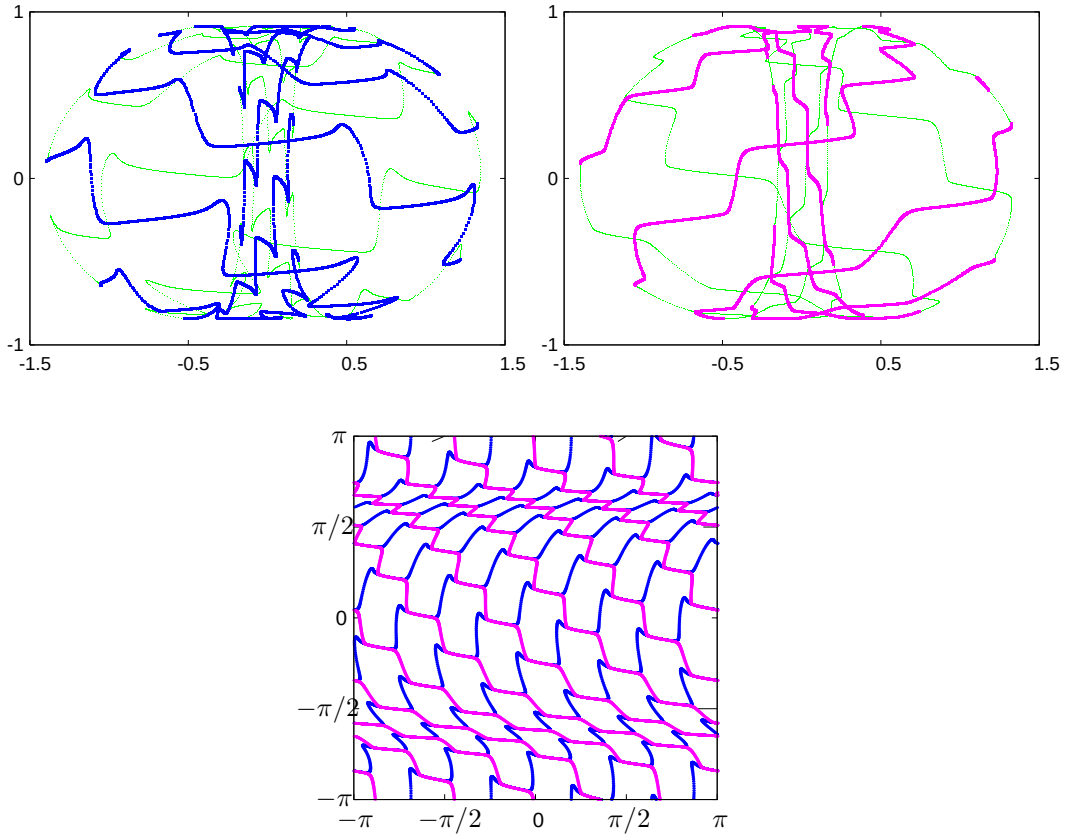

Figure 4: Top left (resp. right): Attracting invariant circle $\mathscr{L}_{a,1}$ (resp. $\mathscr{L}_{a,2}$), occurring for $\omega = 0.219783, \mu = 0.41907$ (resp. same $\omega, \mu = 0.41909$) near the boundary of the large resonance gap in green (resp. in red) close to the black point in Figure 3 bottom. Projection on the (x, z)-plane. The 'front half' of $\mathscr{L}_{a,1}$ (resp. $\mathscr{L}_{a,2}$), *i.e.*, all points (x, y, z) for which $y > 0$, is plotted with blue (resp. magenta) thicker dots, the back half in green. Bottom: Simultaneous projection on a "standard torus" of both invariant circles $\mathscr{L}_{a,1}$ and $\mathscr{L}_{a,2}$. See text.

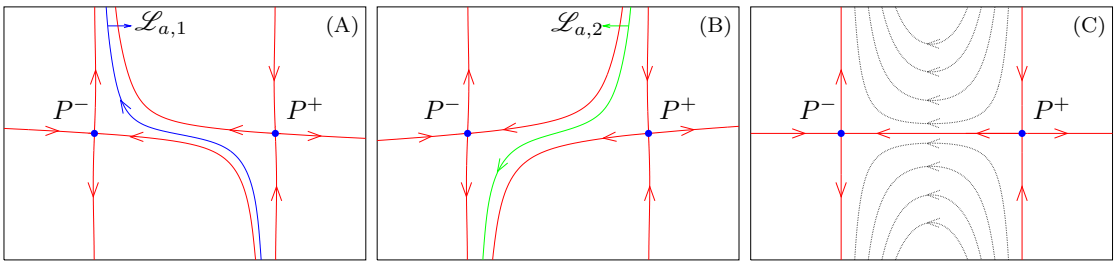

Figure 5: (A) Qualitative sketch of the positions of the attracting invariant circle $\mathscr{L}_{a,1}$ and of the stable and unstable manifolds of the periodic points $P^{\pm}$ inside the two-torus attractor $\mathscr{T}$. (B) Same as (A) for the attracting invariant circle $\mathscr{L}_{a,2}$. (C) Sketch of dynamics for the time-one map of a Hamiltonian vector field on the two-torus $\mathbb{S}^1 \times \mathbb{S}^1$, of which (A) and (B) are perturbations, see text for details.

roughly straight segments of $\mathscr{L}_{a,1}$ and $\mathscr{L}_{a,2}$ lying quite close to each other. According to the explanation proposed above, this is due to the fact that both invariant circles pass through a narrow 'corridor' bounded by the manifolds $W^u(P^+)$ and $W^s(P^-)$, compare Figure 5 (A) and (B). The above scenario is studied by a model map on the two-torus in next section.

4 A simple model map on the two-torus

The simplest possibility to describe dynamics in the two-torus with a double resonance is to take a map with fixed points. The map can be obtained as a perturbation of the time ε flow of a Hamiltonian, e.g. by integrating the flow using Euler's method. We consider $\mathbb{T}^2$ as $[0,1]^2$ modulus 1. A suitable family of Hamiltonian functions is

$$H = \frac{1}{2\pi}(\cos(2\pi x) + (1-\mu)\cos(2\pi y)), \quad \mu \in [0,1) \tag{14}$$

having $(0,0)$ and $(1/2,1/2)$ as elliptic fixed points and $(0,1/2),(1/2,0)$ as saddles. Using the simplest case $\mu = 0$ in (14) presents the problem that the separatrices $x \pm y = 1/2$ are exactly preserved by Euler's method. For $\mu > 0$ they are on different levels of the energy. To "move the separatrices" so that they become close for the flow (and, hence, for the map) one can use the classical trick of "rotated planar vector fields". That is, the Hamiltonian vector field is rotated by $2\pi\alpha$ for a suitable value of α. The final map reads

$$\begin{pmatrix} x \\ y \end{pmatrix} \mapsto \begin{pmatrix} x \\ y \end{pmatrix} + \varepsilon \begin{pmatrix} \cos(2\pi\alpha) & -\sin(2\pi\alpha) \\ \sin(2\pi\alpha) & \cos(2\pi\alpha) \end{pmatrix} \begin{pmatrix} -(1-\mu)\sin(2\pi y) \\ \sin(2\pi x) \end{pmatrix} \mod 1. \tag{15}$$

The concrete values $\varepsilon = 0.1, \mu = 0.5$ have been used and α has been taken as free parameter.

A suitable domain for our purpose is $\alpha \in [\alpha_0 \pm 2\times 10^{-8}]$, with $\alpha_0 = -0.0108670402$. Figure 6 displays the maximal Lyapunov exponent ℓ_1 as a function of α in the selected interval. For $\alpha - \alpha_0 < 0$ and not too close to zero, the situation is familiar: for most parameter values there are attracting invariant circles with irrational rotation number, corresponding to $\ell_1 = 0$, and small (dense) gaps associated to resonances, identified by a negative maximal Lyapunov exponent. Three of these invariant circles can be seen in Figure 7 left. They do a full loop (we recall that we are plotting modulo 1 in the vertical direction). The two circles on the sides of the plot exist for $\alpha = -0.00886704$ (that is, at the left of α_0) whereas the third exists for $\alpha = -0.01286704$, at the right of α_0. Of particular interest is the parameter region of transition between the two.

The tiny gaps where $\ell_1 < 0$ on the left of Figure 6 left correspond to attracting periodic orbits of periods $96, 98, 100, \ldots$ (from left to right). The large gap on the left of Figure 6 right corresponds to period 110. Conversely, for $\alpha - \alpha_0 > 0$ and not too close to zero, there are two invariant circles (because of the symmetry of (15)). They cross the square in the vertical direction. The related gaps on Figure 6 left correspond to periods $48, 49, 50, \ldots$. The large gap on the right of Figure 6 right corresponds to period 55.

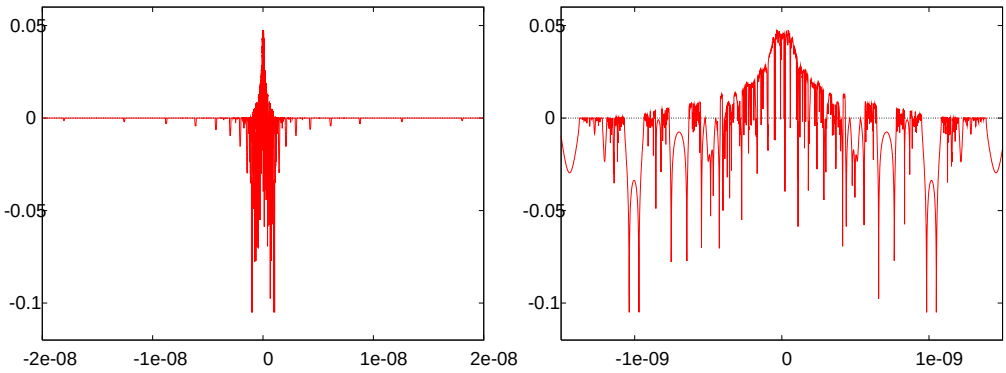

Figure 6: Maximal Lyapunov exponent for (15) as a function of α. In the horizontal axis the value of $\alpha - \alpha_0$ is used. Right: magnification of left plot.

For α close to α_0 the invariant manifolds of the saddle fixed point at $(0, 1/2)$ approach each other and have transversal intersections for some range of α. Moving to the interior of this range the invariant circle, in the passage near the saddle, becomes tangent to the stable foliation of the saddle, for some values of α (one smaller than α_0, the other greater than α_0). From that point on, the circle cannot exist (it would have unbounded length). Then either periodic attractors, or periodic strange attractors or global strange attractors, exist. The situation has many features in common with the scenarios described in [7] and reflects the relevance of the motion of the invariant manifolds as a function of the parameters, as already stressed in [20, 21].

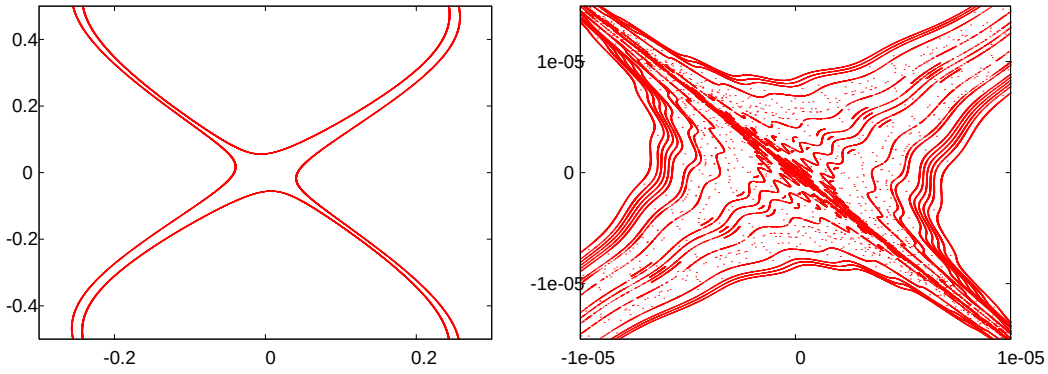

Figure 7: Left: the two curves to the left and right sides of the plot are the invariant circle attractors of (15) for $\alpha = -0.00886704$. The other closed curve is the invariant circle attractor for $\alpha = -0.01286704$.. Right: the attractors of (15) (either invariant circle, periodic orbit or strange attractor) are simultaneously plotted for α varying between -0.010867042 and -0.010867038 with step 10^{-10}. Note that in all these figures we have plotted the variables $(x - 1/2, y)$ to have the saddle fixed point at the origin.

5 Going back to family Q

Finally, guided by the observations of Sec. 4 we would like to see analogous behaviour in the map Q. A suitable place is a neighbourhood of the black point in Figure 3, moving in the horizontal line $\omega = 0.219783$, which is the value used for the invariant circles of Figure 4. However, any attempt to draw a diagram for the maximal Lyapunov exponent ℓ_1, similar to Figure 6, gives estimates very close to zero (say, absolute value less than 10^{-7}, even using 10^9 iterates after some transient).

Looking for the change of resonance associated to the change in the invariant circle between Figure 4 left and right, we have arrived to an interval of width 2×10^{-13} around $\mu = \mu_0 = 0.419081283215$. For that value the observed results are not compatible with the existence of an invariant circle. As before, the computation of ℓ_1 does not allow to draw conclusions on the occurrence of strange attractors. Figure 8 displays the computed attractors for $\mu = \mu_0$ and for $\mu_\pm = \mu_0 \pm 10^{-13}$. Also the representation in the standard two-torus $\mathbb{T}^2$ and a magnification of the projections on (x, y) are displayed (from a total of 10^8 iterates, the fraction falling inside the selected window is roughly 1/600 of the total). From this last picture it is clearly seen that the projection of the attractor for $\mu = \mu_0$ is quite thick. Much more than one can expect from the mere influence of round off errors. A picturesque invariant circle attractor is plotted at the bottom right part of the figure.

To have a better idea of the character of these attractors we have used the following method:

1. Search for a part of the attractor that in some projection is roughly horizontal. Select a suitable window.

2. Compute a large number of iterates (after a transient) only keeping those ones falling inside the window.

3. Fit the data (e.g. y as a function of x) by polynomials of increasing order until no significant reduction of the residual variance is achieved.

4. The residual standard deviation, or the width on the vertical direction of the set of points after subtracting the fitting, gives an idea about how close to a curve is the attractor. One can also check how this standard deviation or width changes as a function of the total number of iterations.

The results for the attractors in Figure 8 are the following. Applying the above method to the attractors in Figure 4, the obtained residual widths are of the order of 10^{-13}, which is a reasonable effect of round off for a large number of iterates. Therefore, these attractors can be quite safely considered as invariant circles. On the other hand, for $\mu = \mu_0$ the observed width is $\approx 2 \times 10^{-3}$. But for μ_- and μ_+ the widths are $\approx 2 \times 10^{-4}$ and $\approx 6 \times 10^{-6}$, respectively. One can conclude that none of these attractors are invariant circles. Therefore, the clear effects of the interaction of resonances (as in the model of Sec. 4) seem to occur here at an extremely narrow scale.

Note that an explanation of the results displayed in Figure 8 requires to take into account round off errors. For the fixed value $\omega = 0.219783$, the range between μ_- and μ_+ has been scanned using step 10^{-15}. To figure out the effect of round off,

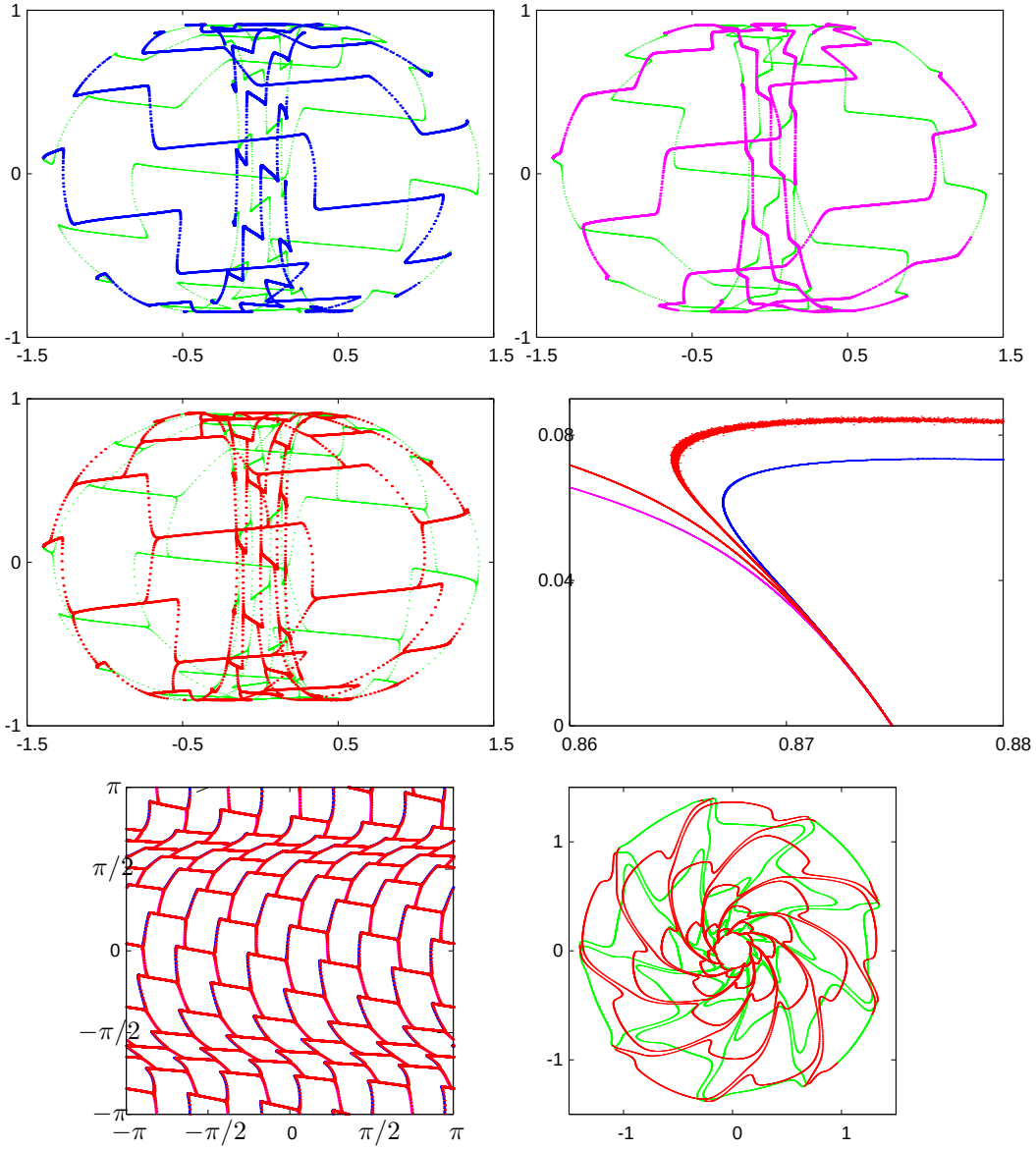

Figure 8: Attractors for Q on $\omega = 0.219783$ and a tiny range in μ around $\mu_0 = 0.419081283215$. Top: the attractors look like invariant circles for $\mu_- = \mu_0 - 10^{-13}$ ($\mathscr{L}_{\mu_-}$, left) and $\mu_+ = \mu_0 + 10^{-13}$ ($\mathscr{L}_{\mu_+}$,right). As in Figure 4 the projection on (x, z) is shown and the thicker points (in blue and magenta) are those with $y > 0$. Middle left: attractor for $\mu = \mu_0$, its front part is plotted in red. This attractor looks like sometimes being close to $\mathscr{L}_{\mu_-}$ other times close to $\mathscr{L}_{\mu_+}$. Middle right: a magnification of a simultaneous projection on the (x, y) plane of the three attractors occurring at μ_-, μ_+, μ_0 (in blue, magenta, and red respectively). Bottom left: a simultaneous projection of the three attractors on the standard torus $\mathbb{T}^2 = [-\pi, \pi]^2$ by the transformation used in Figure 4. The attractor for $\mu = \mu_0$ is plotted after the other two have been plotted and covers them both. Bottom right: a picturesque invariant circle attractor in the resonance $13 : 11 : -3$. Projection on (x, y). In red (resp. green) the points with $z > 0$ (resp. $z < 0$).

several different runs have been done, using computers with different architecture, different languages, different compiling options, and programmes done by different persons. The range in which plots like the one in the middle of Figure 8 (or even more fuzzy) have been obtained is $[\mu_0 - 50 \times 10^{-15}, \mu_0 + 53 \times 10^{-15}]$, with variations in $\pm 10^{-15}$ depending on the run. A reason for that can be that the splitting of the separatrices of the invariant manifolds involved in the creation of chaotic behaviour, when transversal homo/heteroclinic points exist, is of the order of 10^{-13}.

6 Conclusions and future research

The results of the numerical exploration of the model map Q (3) agree very well with the theoretical expectations, based on standard and quasi-periodic bifurcation theory and normal hyperbolicity, discussed at the end of Sec. 2. However, the present exploration reveals many intricate phenomena, that can only be understood by means of further specific investigation. A particularly rich bifurcation structure is detected near crossings of (multiple) resonance gaps. Near some of the wider gap crossings strange attractors appear (see Figure 2, bottom panel). It is still unclear whether the two-torus $\mathscr{T}$ breaks down in this case. Heteroclinic bifurcations of saddle periodic points, taking place inside the two-torus, are conjectured to occur in the transition between nearby resonance gaps. This might provide a route for the creation of a strange attractor contained inside the two-dimensional surface of the normally hyperbolic two-torus; therefore, this would constitute the first concrete example of the Newhouse-Ruelle-Takens scenario [18, 19]. A future project here is to identify in map Q the dynamical phenomena observed in the model map of the two-torus discussed in Sec. 4. We also foresee that new phenomena are likely to occur.

Acknowledgements

The authors are indebted to Enric Castellà, Angel Jorba, Robert Roussarie and Joan Carles Tatjer for help and suggestions and thank the respective institutions for kind hospitality. C.S. has been supported by grants MTM2006-05849/Consolider (Spain) and CIRIT 2005 SGR-1028 (Catalonia).

References

[1] V.I. Arnol'd: *Geometrical Methods in the Theory of Ordinary Differential Equations (2nd ed.)*, Springer–Verlag (1988).

[2] C. Baesens, J. Guckenheimer, S. Kim, R.S. McKay: Three coupled oscillators: mode-locking, global bifurcations and toroidal chaos, *Phys. D* **49(3)** (1991), 387–475.

[3] H.W. Broer, G.B. Huitema, M.B. Sevryuk: *Quasi-periodic Motions in Families of Dynamical Systems, Order amidst Chaos*, Springer LNM **1645** (1996).

[4] H.W. Broer, G.B. Huitema, F. Takens, B.L.J. Braaksma: Unfoldings and bifurcations of quasi-periodic tori, *Mem. AMS* **83(421)** (1990), 1–175.

[5] C. Simó, H.W. Broer, R. Roussarie: A numerical exploration of the Takens-Bogdanov bifurcation for diffeomorphisms, in *European Conference on Iteration Theory (ECIT 89), Batschuns (Austria)*, C. Mira, N. Netzer, C. Simó and G. Targonski, editors, 320–334, World Scientific, Singapore, 1991.

[6] H.W. Broer, R. Roussarie, C. Simó: Invariant circles in the Bogdanov-Takens bifurcation for diffeomorphisms, *Ergod. Th. & Dynam. Sys.* **16** (1996), 1147–1172.

[7] H.W. Broer, C. Simó, J.C. Tatjer: Towards global models near homoclinic tangencies of dissipative diffeomorphisms, *Nonlinearity*, **11**(3) (1998), 667–770.

[8] H.W. Broer, C. Simó, R. Vitolo: The Hopf-saddle-node bifurcation for fixed points of 3D-diffeomorphisms: analysis of a resonance 'bubble', *Physica D* **237(13)** (2008), 1773–1799.

[9] H.W. Broer, C. Simó, R. Vitolo: The Hopf-saddle-node bifurcation for fixed points of 3D-diffeomorphisms: a computer assisted dynamical inventory, *in preparation* (2007).

[10] H.W. Broer, F. Takens, F.O.O. Wagener: Integrable and non-integrable deformations of the skew Hopf bifurcation, *Regular and Chaotic Dynamics* **4(2)** (1999), 17–43.

[11] A. Chenciner: Bifurcations de points fixes elliptiques. I. Courbes invariantes, *Publ. Math. IHES* **61** (1985), 67–127.

[12] A. Chenciner: Bifurcations de points fixes elliptiques. II. Orbites périodiques et ensembles de Cantor invariants, *Invent. Math.* **80** (1985), 81–106.

[13] A. Chenciner: Bifurcations de points fixes elliptiques. III. Orbites périodiques de "petites" périodes et élimination résonnante des couples de courbes invariantes, *Publ. Math. IHES* **66** (1987), 5–91.

[14] Yu. Kuznetsov: *Elements of Applied Bifurcation Theory* (2nd ed.), Springer–Verlag (1998).

[15] Yu. Kuznetsov, H.G.E. Meijer: Remarks on interacting Neimark-Sacker bifurcations, *Journal of Difference Equations and Applications* **12(10)** (2006), 1009–1035.

[16] Yu. Kuznetsov, H.G.E. Meijer, and L. van Veen: The fold-flip bifurcation, *IJBC* **14(7)** (2004), 2253–2282.

[17] H.G.E. Meijer: *Codimension 2 Bifurcations of Iterated Maps*, PhD thesis, University of Utrecht (2006).

[18] S. Newhouse, D. Ruelle, F. Takens: Occurrence of strange Axiom A attractors near quasiperiodic flows on $\mathbb{T}^m$, $m \geq 3$, *Comm. Math. Phys.* **64** (1978), 35–40.

[19] D. Ruelle, F. Takens: On the nature of turbulence, *Comm. Math. Phys.* **20** (1971), 167–192.

[20] C. Simó: On the Hénon-Pomeau attractor, *J. of Statistical Physics*, **21** (1979), 465–494.

[21] C. Simó: Some experiments with planar maps: strange attractor, stable zones and the role of unstable invariant manifolds, in *Nonlinear Problems of Analysis in Geometry and Mechanics*, M. Atteia, D. Bancel and I. Gumowski, editors, *Res. Notes in Math.* **46**, 176–183, Pitman, 1981.

[22] C. Simó: Perturbations of translations in the two-dimensional torus: the case near resonance. *Actas VI CEDYA*, Universidad de Zaragoza, (1984).

[23] C. Simó: Global Dynamics and Fast Indicators, in *Global Analysis of Dynamical Systems*, H. W. Broer, B. Krauskopf, G. Vegter, editors, 373–390, IOP Publishing, Bristol, 2001.

[24] F. Takens: Forced oscillations and bifurcations, in *Applications of Global Analysis* **1** (1974), Communications of the Mathematical Institute Rijksuniversiteit Utrecht **3**, reprinted in *Global analysis of dynamical systems: Festschrift dedicated to Floris Takens for his 60th birthday* (H.W. Broer, B. Krauskopf, and G. Vegter Eds.), IOP Publish., Bristol (2001).

[25] F. Takens, F.O.O. Wagener: Resonances in skew and reducible quasi-periodic Hopf bifurcations, *Nonlinearity* **13(2)** (2000), 377–396.

[26] R. Vitolo: *Bifurcations of attractors in 3D diffeomorphisms*, PhD thesis, University of Groningen (2003).

[27] F.O.O. Wagener: Semi-local analysis of the k:1 and k:2 resonances in quasi-periodically forced systems, in *Global analysis of dynamical systems. Festschrift dedicated to Floris Takens for his 60th birthday* (H.W. Broer, B. Krauskopf, G. Vegter eds.), IOP, Bristol and Philadelphia (2001), 113–129

[28] F.O.O. Wagener: On the skew Hopf bifurcation, PhD Thesis, University of Groningen (1998).

H. W. Broer
Dept. of Mathematics, Univ. of Groningen
P.O. box 407, 9700 AK Groningen
The Netherlands
Tel: +31 (0)50 363 3959 (3939)
Fax: +31 (0)50 363 3800
email: broer@math.rug.nl

C. Simó
Departament de Matemàtica Aplicada i Anàlisi, Universitat de Barcelona
Gran Via 585, 08007 Barcelona
Spain
Tel: +34 93 402 1641 (1650)
Fax: +34 93 402 1601
email: carles@maia.ub.es

R. Vitolo
School of Engineering, Computing and Mathematics
University of Exeter, Harrison building, room 319
North Park Road, EXETER, EX4 4QF
email: renato.vitolo@unicam.it, R.Vitolo@exeter.ac.uk